ISSN 2229-5518

The Modeling and Simulation of a Microturbine Generation System

Godswill Ofualagba

Abstract— In a hybrid energy system consisting of renewable sources of energy, there should be some storage facility or backup generation to maintain continuity of supply to the load when renewable source alone is not sufficient. The objective of this paper is to present one of such generating system that is capable of acting as a backup generator. This paper presents the modeling and simulation of a microturbine generation (MTG) system, the nonrenewable source of energy suitable for isolated as well as grid-connected operation. The system comprises of a permanent magnet synchronous generator driven by a microturbine. A brief description of the overall system is given and mathematical models for the microturbine and permanent magnet synchronous generator are presented. The developed models are simulated in MATLAB/Simulink.

Index Terms— Acceleration control, fuel system, compressor-turbine, machine, microturbine generation system (MTG), temperature control, permanent magnet synchronous generator.

1 INTRODUCTION

MTG systems are gaining popularity in distributed power generation because of their smaller size, high efficiency (with recuperator), and faster response compared to the conventional gas turbines. Microturbines are capable of burning a number of fuels at high and low pressure levels, including natural gas, waste (sour) gas, landfill gas, or propane. Today's microturbine technology is the result of the development work, in small stationary and automotive gas turbines, pursued by the automotive industry beginning in the 1950's. As a result of which, modern microturbines are able to combine the reliability of on board commercial aircraft generators with the low cost of automotive turbochargers.

This paper presents the modeling and simulation of a microturbine generation (MTG) system, the nonrenewable source of energy suitable for isolated as well as grid-connected operation. The system comprises of a permanent magnet synchronous generator driven by a microturbine. A brief description of the overall system is given and mathematical models for the microturbine and permanent magnet synchronous generator are presented.

In the last section of this paper, the developed models are simulated in MATLAB/Simulink. The simulated microturbine model is of single shaft type with control systems capable of regulating its output power. Simulation results are presented
for the developed model of the MTG system under different load conditions.

2 MICROTURBINE GENERATION (MTG) SYSTEM

Microturbines are small gas turbines which burn gaseous or liquid fuels to create high energy gas stream that turns an electrical generator. There is a growing interest in the application of MTGs as they can start quickly and are especially useful for on-peak power supply for grid support. Other applications include remote power and combined heat and power (CHP) systems by utilizing the heat contained in the exhaust gases to supply thermal energy needs in a building or industrial process [1]-[4].

Generally MTG systems range from 30 to 400 kilowatts [11]-[13], while conventional gas turbines range from 500 kW to more than 300 MW [9], [10]. Microturbines are capable of burring a number of fuels at high and low pressure levels. They generally have marginally lower electrical efficiencies than similarly sized reciprocating engine generators. Without a recuperator the overall efficiency of a microturbine is 15 to 17%, where as with an 85% effective recuperator the efficiency can be as high as 33 to 37% [13]. However, because of their design simplicity and relatively fewer moving parts, microturbines have the potential for simpler installation, higher reliability, reduced noise and vibration, lower maintenance requirements, lower emissions, continuous combustion and possibly lower capital costs compared to reciprocating engines [1], [4], [12]. Microturbines emissions can be up to eight times lower than diesel generators, and currently available ones produce less than 50% of the NOx emissions of a state of the art natural gas lean-burn engine [1].

2.1 Types of Microturbine Systems

There are mainly two types of microturbine systems available, single-shaft models and two shaft models. In single-shaft designs, a single expansion turbine turns both the compressor and the generator. As a result they operate at high-speeds, some in excess of 100,000 rpm, and generate electrical power at high frequency (in the order of kHz). Two-shaft models on the other hand, uses a turbine to drive the compressor on one shaft and a power turbine on a separate shaft connected to a conventional generator via a gear box which generates AC power at 60 Hz or 50 Hz [17]. In a single-shaft design, since the generator provides a high frequency AC voltage source, a power electronic interface between the MTG system and the AC load is required. For a two-shaft design, on the other hand, there is no need for such interfacing. This paper considers the modeling single-shaft type only.

• *Godswill Ofualagba is a lecturer at Federal University of Petroleum Resources, Department of Electrical and Electronics Engineering, Effurun, Nigeria. E-mail: swillas@ieee.org*

2.2 Basic Process and Components of a MTG System

The basic components of a microturbine generation system are: compressor, turbine, recuperator, high-speed generator and power electronics interfacing. In the following paragraphs a brief description of each component is given, followed by a detailed modeling of microturbine and high-speed generator. Figure 4.1 shows the schematic diagram of a single-shaft microturbine based generation system [1], [5].

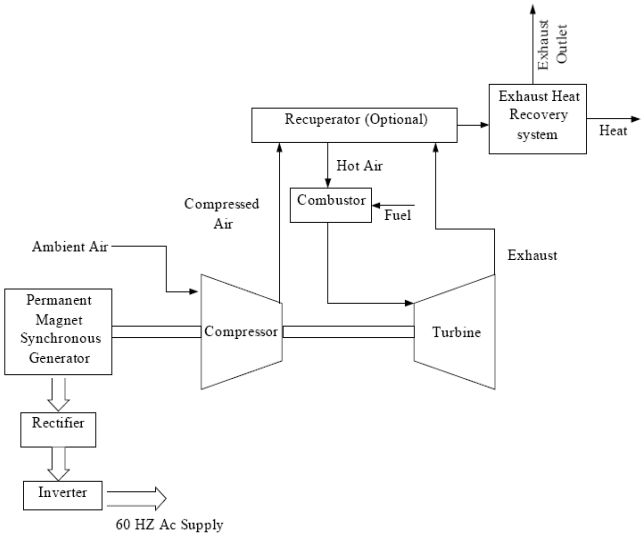

Fig.1 Microturbine based CHP system (Single-Shaft Design).

Microturbines, like large gas turbines, operate based on the thermodynamic cycle known as the Brayton cycle [1]. In this cycle, the inlet air is compressed in a radial (or centrifugal) compressor. The compressed air is mixed with fuel in the combustor and burned. The hot combustion gas is then expanded in the turbine section, producing rotating mechanical power to drive the compressor and the electric generator, mounted on the same shaft (single-shaft design). In a typical microturbine air to gas heat exchanger called recuperator is added to increase the overall efficiency. The recuperator uses the heat energy available in the turbine's hot exhaust gas to preheat the compressed air before the compressed air goes into the combustion chamber thereby reducing the fuel needed during the combustion process.

The high-speed generator of the single shaft design usually employs a permanent magnet synchronous generator (PMSG), and requires that the high frequency AC output in the order of kHz be converted to 60 Hz (or 50 Hz) for general use. This power conditioning involves rectifying the high frequency AC to DC and then inverting the DC to 60 Hz (or 50 Hz) AC. Power electronic interfacing is a critical component in the single-shaft design and is generally designed to handle transient and voltage spikes [1].

The model presented in this thesis concentrates on the slow dynamics of the MTG system, suitable for power management of MTG combined with other types of distributed generation (DG) systems. It is reasonable, while modeling the microturbine for the above purpose, to assume that the system is operating under normal operating conditions by neglecting fast dynamics of the microturbine (e.g., start-up, shutdown, internal faults and loss of power). Also, since the electromechanical behavior of the MTG system is of main interest the recuperator is not included in the model as it only serves to increase the turbine efficiency [17].

3 Mathematical Representation of a Microturbine

There exists a large literature on the modeling of gas turbines, with varying level of complexity depending on the intended application. The concept of gas turbine system presented in this section is based on the paper presented by Rowen [6]. He proposed a single-shaft design, generator driven gas turbine model which includes speed control, temperature control and fuel system. This model was successfully adopted by the several authors for gas turbine simulations [7]-[10] as well as for microturbine simulations with smaller time constants [11], [12].

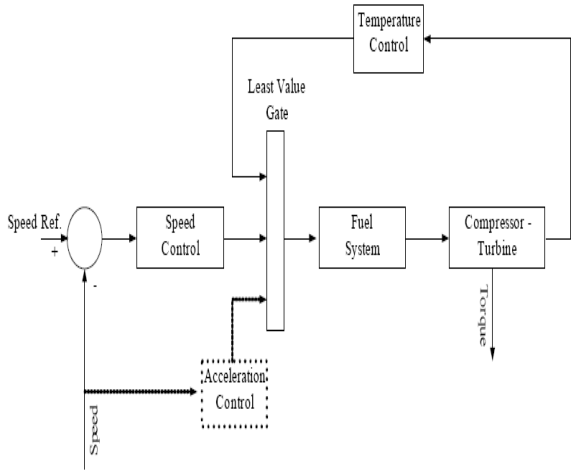

Fig. 2 Block diagram of a microturbine.

The three control functions of the microturbine are: speed control acting under part load conditions, temperature control acting as an upper output power limit, and acceleration control to prevent over speeding. The output of these control function blocks
are all inputs to a least value gate (LVG), whose output is the lowest of the three inputs and results in the least amount of fuel to the compressor-turbine as shown in Figure 2. This figure shows the per-unit representation of a microturbine, along with its control systems [6]. Each subsystem of the microturbine is discussed in the following subsections.

3.1 Speed and Acceleration Control

The speed control operates on the speed error formed between a reference (one per-unit) speed and the MTG system rotor speed. It is the primary means of control for the microturbine under part load conditions. Speed control is usually modeled by using a lead-lag transfer function [6], or by a PID controller [8]. In this work a lead lag transfer function has been used to represent the speed controller, as shown in Figure 3. In this figure K is the controller gain, T1 (T2) is the governor lead (lag) time constant, and Z is a constant

representing the governor mode (droop or isochronous). A droop governor is a straight proportional speed controller in which the output is proportional to the speed error. An isochronous speed controller is a proportional-plus-reset speed controller in which the rate of change of the output is proportional to the speed error.

Acceleration control is used primarily during turbine startup to limit the rate of the rotor acceleration prior to reaching operating speed. If the operating speed of the system is close to its rated speed, the acceleration control could be eliminated in the modeling [6], which is the case in this study.

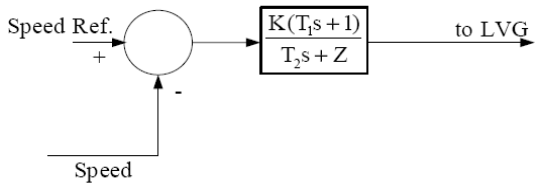

Fig.3 Speed controller for the microturbine.

3.2 Fuel System

The fuel system consists of the fuel valve and actuator. The fuel flow out from the fuel system results from the inertia of the fuel system actuator and of the valve positioner [6], [8], whose equations are given below.

The valve positioner transfer function is:

$$E_1 = \frac{K_v}{T_v s + c} F_d \qquad (1)$$

and the fuel system actuator transfer function is:

$$Wf = \frac{K_f}{T_f s + c} E_1 \qquad (2)$$

In (1) and (2), K_v, K_f is the valve positioner (fuel system actuator) gain, T_v ,T_f are the valve positioner and fuel system actuator time constants, c is a constant, F_d and E_1 are the input and outputs of the valve positioner and W_f is the fuel demand signal in p.u.

The output of the LVG, V_{ce}, represents the least amount of fuel needed for that particular operating point and is an input to the fuel system. Another input to the fuel system is the per-unit turbine speed N (limited by the acceleration control). The per-unit value for V_{ce} corresponds directly to the per-unit value of the mechanical power on turbine at steady-state. The fuel flow control as a function of *Vce* is shown in Figure 4.

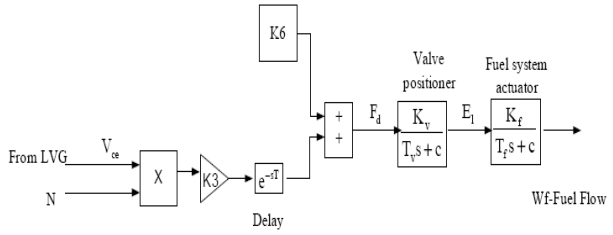

Fig.4 Block diagram of the fuel system

The value of V_{ce} is scaled by the gain *K3* (*K3= (1-K6)*), then delayed and offset by the minimum amount of fuel flow *K6* to ensure continuous combustion process in the combustion chamber. *K6* is essentially the minimum amount of fuel flow at no-load, rated speed.

3.3 Compressor-Turbine

The compressor-turbine is the heart of the microturbine and is essentially a linear, nondynamic device (with the exception of the rotor time constant) [6]. There is a small transport delay T_{CR}, associated with the combustion reaction time, a time lag T_{CD}, associated with the compressor discharge volume and a transport delay T_{TD} , for transport of gas from the combustion system through the turbine. The block diagram of the compressor-turbine package is shown in Fig. 5. In this figure both the torque and the exhaust temperature characteristics of the single-shaft gas turbine are essentially linear with respect to fuel flow and turbine speed and are given by the following equations [6]:

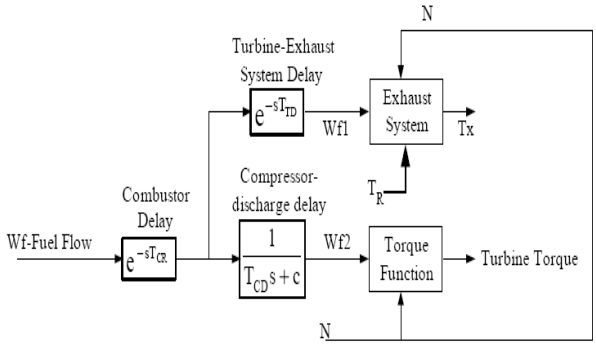

Fig. 5 Compressor-Turbine package of a microturbine

$$Torque = K_{HHV}(W_{f2}-0.23)+0.5(1-N)\ (Nm) \qquad (3)$$

$$Exhaust\ Temp.,\ Tx = T_R-700(1-W_{f1})+550(1-N)\ (^{\circ}F) \qquad (4)$$

where K_{HHV} is a coefficient which depends on the enthalpy or higher heating value of the gas stream in the combustion chamber and T_R is the reference temperature [6], [9]. The K_{HHV} and the constant 0.23 in the torque expression cater for the typical power/fuel rate characteristic, which rises linearly from zero power at 23% fuel rate to the rated output at 100% fuel rate.

The input to this subsystem is the p.u. fuel demand signal W_f and outputs are the p.u. turbine torque and exhaust temperature (°F).

3.4 Temperature Control

Temperature control is the normal means of limiting the gas turbine output power at a predetermined firing temperature, independent of variation in ambient temperature or fuel characteristics. The fuel burned in the combustor results in turbine torque and in exhaust gas temperature. The exhaust temperature is measured using a series of thermocouples incorporating radiation shields as shown in the block diagram of the temperature controller (Fig. 6). In Fig. 6, T_t is the temperature controller integration rate and T_3, T_4 are time constants associated with the radiation shield and thermocouple, respectively. K_4 and K_5 are constants associated with radiation shield and T_5 is the time constant associated with

temperature controller. The output from the thermocouple is compared with a reference temperature, which is normally higher than the thermocouple output. This forces the output of the temperature control to stay on the maximum limit permitting the dominance of speed control through the LVG (Fig. 2). When the thermocouple output exceeds the reference temperature, the difference becomes negative, and the temperature control output starts decreasing. When this signal (Fig. 2) becomes lower than the speed controller output, the former value will pass through the LVG to limit the turbine's output, and the turbine operates on temperature control. The input to the temperature controller is the exhaust temperature (*Tx*) and the output is the temperature control signal to the LVG [6], [9].

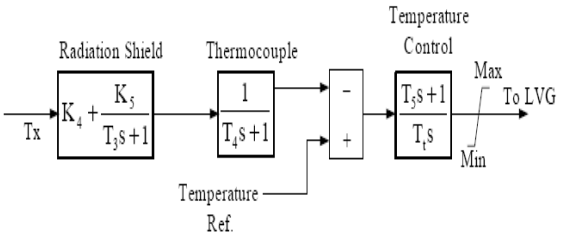

Fig. 6 Temperature controller.

4 PERMANENT MAGNET SYNCHRONOUS GENERATOR (PMSG)

Microturbine produces electrical power via a high-speed generator directly driven by he turbo-compressor shaft. Small gas turbines benefit in particular when the gearbox that reduces the shaft speed to the speed of conventional electrical machines is eliminated, as is the case with the single-shaft designs considered here. The result is a more efficient, compact and reliable machine and the shaft speed is normally above 30,000 rev/min and may exceed 100,000 rev/min. High energy permanent magnets and high yield-strength materials like neodymium-iron-boron (NdBFe) or Samarium-cobalt magnets have proved very suitable for high-speed electrical machines [1], [5].

In the following sections the equivalent circuit of a permanent magnet synchronous machine (PMSM) is presented along with a brief description of its construction, operation and the permanent magnet materials.

In a permanent magnet synchronous machine, the dc field winding of the rotor is replaced by a permanent magnet. The advantages are elimination of filed copper loss, higher power density, lower rotor inertia, and more robust construction of the rotor. The drawbacks are loss of flexibility of field flux control and possible demagnetization. The machine has higher efficiency than an induction machine, but generally its cost is higher [15].

4.1 Permanent Magnet Materials

The property of a permanent magnet and the selection of the proper materials are very important in the design of a permanent magnet synchronous machine (PMSM). A good permanent magnet should produce a high magnetic field with a low mass, and should be stable against the influences which would demagnetize it. The desirable properties of such magnets are typically stated in terms of the remanence and coercivity of the materials, and are quoted in Tesla, the basic unit for magnetic field B.

Iron, nickel, cobalt and some of the rare earth metals exhibit a unique magnetic behavior which is called ferromagnetism. Ferromagnets tend to stay magnetized to some extent after being subjected to an external magnetic field. The fraction of the saturation magnetization retained (remanence) when the driving filed is removed is an important factor for the selection of the permanent magnets. All ferromagnetic materials have a maximum temperature known as Curie temperature, where the ferromagnetic property disappears. Consequently, the range of temperatures plays an important role in the operation of a PMSM [14].

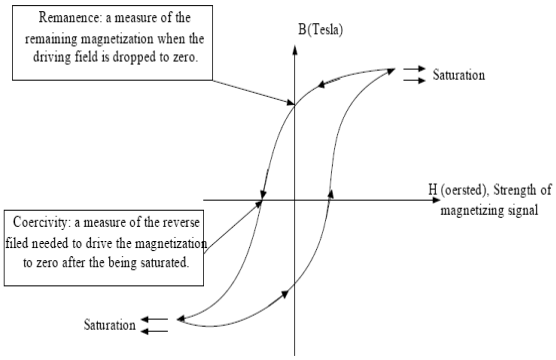

Fig. 7 Hysteresis loop in the form of magnetization B and magnetic field strength H.

4.2 Operating Region of a PMSM

Figure 8 shows the demagnetization segment of the B-H curve where the permanent magnet is usually designed to operate [15].

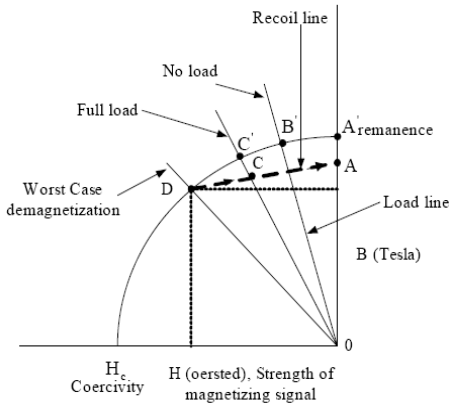

Figure 8 Permanent magnet machine operating points on B-H curve.

The maximum flux density Br corresponding to A ' will be available initially (no airgap). When the magnet is installed in the machine, the air gap will have some demagnetization effect and the operating point B' will correspond to the no-load line as shown in Fig 8. When current flows in the stator winding, the magnetic axis (direct axis) armature reaction effect can have further demagnetization effect, which will reduce the air gap flux density further. A load line representing worst-case demagnetization (may

be due to starting, transient or machine fault condition) is also shown in Figure .8. Once the operating point reaches the D and the demagnetization effect is removed, the magnet will recover along the recoil line (DA). Subsequently, the stable operating point will be determined by the intersection of the load line and the recoil line. The magnet is therefore permanently demagnetized at no-load operation, corresponding to the vertical distance between A' and A. If the permanent magnet material has a straight-line demagnetization curve, the recoil line will coincide with the demagnetization line irrespective of the worst case magnetization point (i.e., permanent demagnetization will be negligible). The characteristics for several possible permanent magnet materials are
given in reference [15].

4.3 dq Axis Representation of a PMSM

In a PMSM, the permanent magnets are glued on the rotor in surface sinusoidal magnet machine (SPM), and are mounted inside the rotor in case of an interior or buried magnet synchronous machine (IPM). The stator has three- phase sinusoidal winding, which creates a synchronously rotating air gap flux. If the machine is rotated by a prime mover, the stator windings generate balanced three-phase sinusoidal voltages. The dq axis representation of a permanent magnet synchronous machine (for a balanced system the 0-axis quantities are equal to zero), where is shown in the Figure 9 [15], [16], [18]. In this figure the finite core loss is represented by the dotted damper windings.

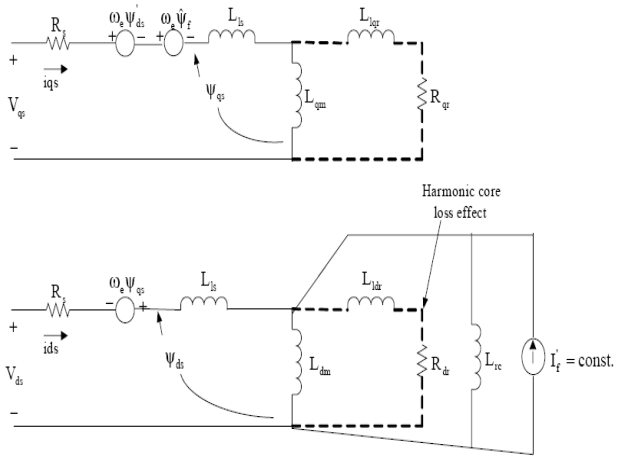

Fig. 9 Synchronously rotating frame equivalent circuits of a PMSM.

Ignoring core loss, the circuit equations can be written as (equations are valid for both IPM as well as SPM (for SPM L_{dm}=L_{qm}):

$$V_{qs} = R_s i_{qs} + \omega_e \psi'_{ds} + \omega_e \hat{\psi}_f + \frac{d\psi_{qs}}{dt} \quad (5)$$

$$V_{ds} = R_s i_{ds} - \omega_e \psi_{qs} + \frac{d\psi_{ds}}{dt} \quad (6)$$

where the flux linkages are given by the following equations:

$$\hat{\psi}_f = L_{dm} I'_f \quad (7)$$

$$\psi'_{ds} = i_{ds}(L_{ls} + L_{dm}) = i_{ds} L_{ds} \quad (8)$$

$$\psi_{ds} = \hat{\psi}_f + \psi'_{ds} \quad (9)$$

$$\psi_{qs} = i_{qs}(L_{ls} + L_{qm}) = i_{qs} L_{qs} \quad (10)$$

The electromagnetic developed in the machine air gap is given by:

$$T_e = \frac{3}{2} \times \frac{P}{2} (\psi_{ds} i_{qs} - \psi_{qs} i_{ds}) \quad (11)$$

Substituting (5)-(8) in (3), (4) and (9) and simplifying, we have

$$\frac{di_{qs}}{dt} = \frac{1}{L_{qs}} \left[V_{qs} - R_s i_{qs} - L_{ds} \omega_e i_{ds} - \hat{\psi}_f \omega_e \right] \quad (12)$$

$$\frac{di_{ds}}{dt} = \frac{1}{L_{ds}} \left[V_{ds} - R_s i_{ds} + \omega_e L_{qs} i_{qs} \right] \quad (13)$$

$$T_e = \frac{3P}{4} [\hat{\psi}_f i_{qs} + (L_{ds} - L_{qs}) i_{qs} i_{ds}] \quad (14)$$

The rotor speed is obtained from the dynamics of the mechanical system as follows:

$$\frac{d\omega_r}{dt} = \frac{1}{J} (T_e - T_{shaft}) \quad (15)$$

where ωe ,ωr are electrical and mechanical angular velocities of the rotor (rad/sec), V_{qs}, V_{ds} (I_{qs}, I_{ds}) are q and d axis voltage (current) components and Lqs and Lds are q and d axis inductances of the stator respectively. Ldm is the common d-axis mutual inductance of the stator lumped with the damper windings and the permanent magnet inductance L_{rc} (associated with the recoil slope).

I_f is an equivalent field current of the permanent magnets and I'_f is its equivalent ref to the stator side,

Ψ_f ($\psi_f = L_{dm} I'_f$ = constant) denotes flux linkage induced by the permanent magnets of the rotor in stator phases,

J is the inertia of the rotor (Kgm^2),

T_{shaft} is the shaft torque produced by the microturbine (Nm),

T_e is the electric torque generated by the PMSG (Nm), and

P is the number of poles.

Note that the signs for the generated torque Te and shaft torque T_{shaft} are positive for motor operation and negative for generator operation.

5 Simulation Results

A mathematical model of the microturbine as explained in the previous section is built in MATLAB/Simulink using SimPowerSystems blockset. An inbuilt model of the permanent magnet synchronous machine in the SimPowerSystems blockset, based on (12)-(15), is used to simulate the PMSG by applying negative torque to the model. All the parameters values used for the simulation are given below. The block diagram of the simulated MTG system is given in Figure 4.10 followed by the simulation results for different operating conditions.

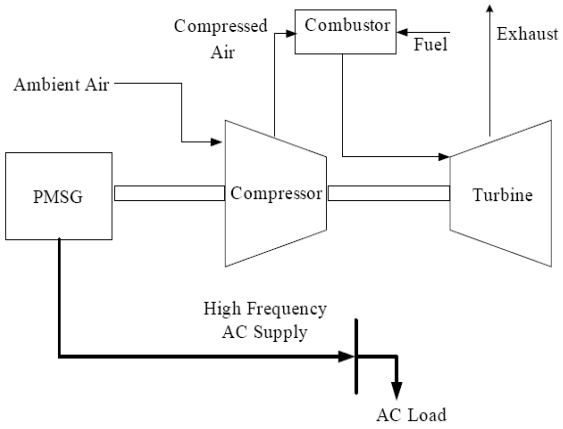

Fig. 10 Block diagram of the simulated MTG system

Parameters are obtained form [6], [9], [10], and adopted for this simulation. All time functions are in seconds.

Microturbine ratings: 400 kW, 70000 rpm.

Speed controller parameters (Fig. 3):
$K=25, T_1=0.4, T_2=1.0, Z=3.$

Fuel system parameters (Fig. 4):
$K_v=1, T_v=0.05, c=1, K_3=0.77, K_6=0.23, K_f=1, T=0, T_f=0.04.$

Compressor-turbine combination parameters (Fig. 5):
$T_{CR}=0.01, T_{TD}=0.04, T_{CD}=0.2, K_{HHV}=1.2.$

Temperature controller parameters (Fig. 6):
$K_4=0.8, K_5=0.2, T_3=15, T_4=2.5, T_5=3.3, T_t=450\,^0F, T_R=950\,^0F.$

Parameters used for the PMSG simulation [4], [18].
$Rs=12.5m$ Ohms, $L_d=L_q=165e\text{-}6$ Henrys, $\Psi_f=0.2388$ wb, $P=4$, $J=0.011$ kg m^2.

Speed reference was kept constant at 1 p.u. for all simulations. All values are referred to a base power rating of 1 MVA. The response of the developed MTG system is given in the following simulation results:

Initially the system is operating at no-load. At t =10 seconds a load of 200kW is applied on the MTG system, and at t = 15 seconds, the load is increased to 400 kW. Figure 11 shows the output power of the MTG system, responding to the above load variations. Figure 12 shows the fuel consumed by the microturbine for the applied load conditions. The fuel demand is equal to 23% (0.23 p.u.) until the load is applied on the system at t=10 seconds, increasing the amount of fuel required to keep the combustion process alive. Note that the fuel demand signal is 0.62 p.u. at 200kW load and increasing to 1 p.u. at full load (400kW).

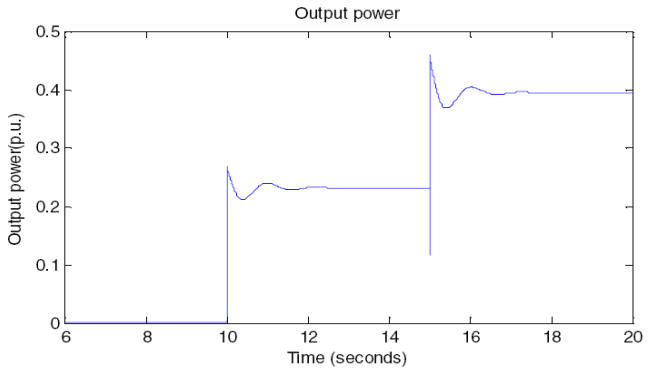

Fig. 11 Power output from the MTG system.

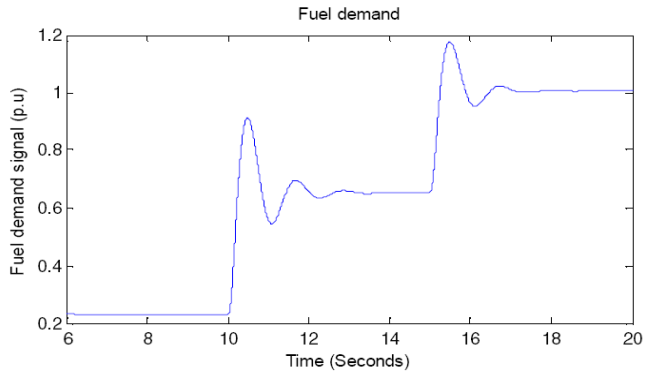

Figure 12 Fuel demand signal of the microturbine.

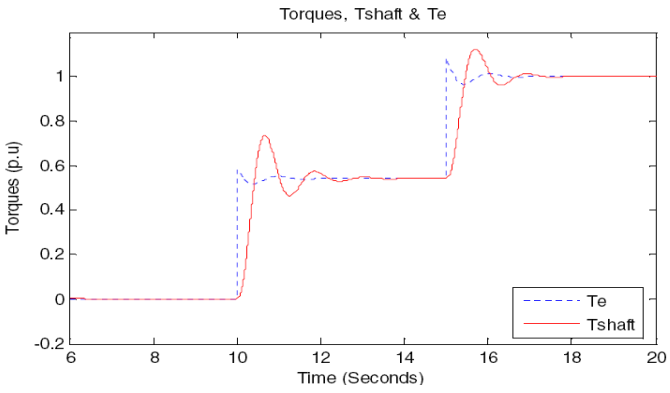

Fig. 13 Variation of shaft torque and electric torque generated

Figure 13 shows the shaft torque (T_{shaft}) produced by the microturbine, which drives the PMSG, and the electromagnetic torque (T_e) generated by the PMSG. The generator torque is approximately same as the shaft torque produced by microturbine at steady- state. At no-load the electromagnetic torque is equal to zero; it increases to about 50% of its base value at 200kW and to 1 p.u. at full load.

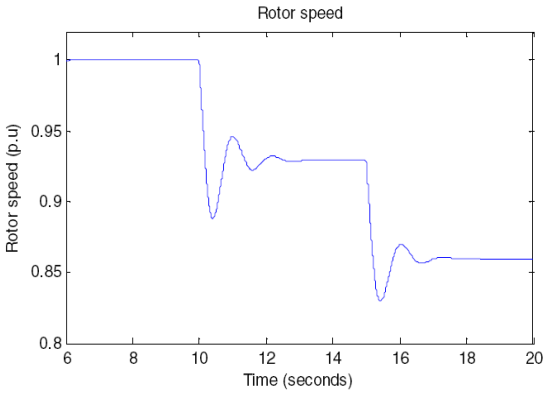

Fig. 14 Rotor speed variations with load.

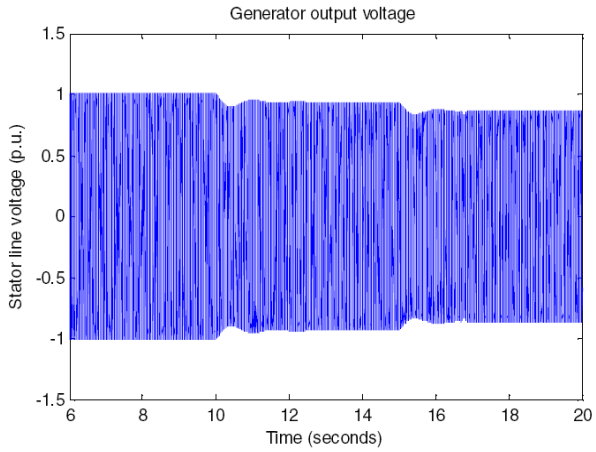

Fig. 15 Voltage across the stator terminals of PMSG.

Figures 14 and 15 show the rotor speed and output voltage of the PMSG. When the MTG is operating at no-load, the speed of the rotor is equal to 1 p.u. and the stator line voltage of the PMSG reaches no-load steady-state value of 1.p.u. (1p.u.=6000 volts peak, Figure 15). When the PMSG is loaded at t =10 seconds, the voltage decreases from no-load value to 0.94 p.u. and the frequency of the voltage waveform decreases from 2.33 kHz to 2.17 kHz. At t=15 seconds, as the load is increased again, the rotor speed (Figure 14) and the stator voltage decrease further to 0.86 p.u. and 0.865 p.u., respectively.

CONCLUSION

The modeling of a single-shaft microturbine generation system suitable for power management in DG applications is presented in this chapter. The model is good for both, power only and CHP applications. Detailed mathematical modeling of the control systems of the microturbine is given and simulation of the developed MTG system model is carried out. A MATLAB/Simulink model of the proposed MTG system was implemented in the SimPowerSystems blockset. Different load conditions are applied on the MTG system. The simulation results show that the developed model of the MTG system has the ability to meet the power requirements of the load, within MTG's rating.

REFERENCES

[1] Larry Goldstein, Bruce Hedman, Dave Knowles, Steven I. Freedman, Richard Woods and Tom Schweizer., "Gas-fired distributed energy resource technology characterizations," National Renewable Energy Laboratory, NREL/TP-620-34783, Nov. 2003.

[2] Robert Lasseter, "Dynamic models for micro-turbines and fuel cells," in Proceedings, IEEE PES Summer Meeting, vol. 2, 2001, pp. 761-766, Jul. 2001, Vancouver, BC, Canada.

[3] Hans B. Puttgen, Paul R. Macgregor and Frank C. Lambert, "Distributed generation: Semantic hype or the dawn of a new era," IEEE Power and Energy Magazine, vol. 1, no. 1, pp. 22-29, Jan. /Feb. 2003.

[4] Anders Malmquist, "Analysis of a gas turbine driven hybrid drive system for heavy vehicles," Ph.D. dissertation, School of Electrical Engineering and Information Technology, KTH, Stockholm, Sweden, 1999.

[5] Anders Malmquist, Ola Aglen, Edgar Keller, Marco Suter and Jari Wickstrom., "Microturbines: Speeding the shift to distributed heat and power," ABB Review, no. 3, pp. 22-30, Mar. 2000.

[6] W. I. Rowen, "Simplified mathematical representations of heavy duty gas turbines", Journal of Engineering for Power, Transactions ASME, vol. 105, no. 4, pp. 865-869, Oct, 1983.

[7] Working Group on Prime Mover and Energy Supply Models for System Dynamic Performance Studies, "Dynamic models for combined cycle plants in power system studies," IEEE Transactions on Power Systems, vol. 9, no. 3, pp. 1698-1708, August 1994.

[8] Francisco Jurado and Jose Ramon Saenz, "Adaptive control of a fuel cell-microturbine hybrid power plant," IEEE Transactions on Energy Conversion, vol. 18 no.2, pp. 342-347, June 2003.

[9] L. N. Hannet and Afzal Khan, "Combustion turbine dynamic model validation from tests," IEEE Transactions on Power Systems, vol. 8, no. 1, pp. 152-158, Feb. 1993.

[10] L. M. Hajagos and G. R. Berube, "Utility experience with gas turbine testing and modeling," in Proceedings, IEEE PES Winter Meeting, vol. 2, 2001, pp. 671-677 Jan. / Feb. 2001, Columbus, OH.

[11] Amer Al-Hinai, Ali Feliachi, "Dynamic model of a microturbine used as a distributed generator," in Proceedings, 34th Southeastern Symposium on system Theory, Huntsville,pp.209-213, Alabama, March 2002.

[12] F. Jurado and A. Cano, "Use of ARX algorithms for modeling micro-turbines on the distribution feeder," in IEE Proceedings: Generation Transmission and Distribution, vol. 151, no. 2, pp. 232-238, Mar. 2004.

[13] Anne-Marie Borbely and Jan F. Kreider, Distributed Generation-The Power Paradigm for the new millennium, CRC Press, 2001.

[14] Web link:
http://hyperphysics.phy-astr.gsu.edu/hbase/solids/magperm.html

[15] Bimal K.Bose, Modern Power Electronics and AC Drives, Pearson Education, 2003.

[16] Chee-Mun Ong, Dynamic Simulation of Electric Machinery, Prentice Hall, 1998.

[17] Y. Zhu and K. Tomsovic, "Development of models for analyzing the load-following performance of microturbines and fuel cells," Journal of Electric Power Systems Research, vol. 62, pp. 1-11, 2002.

[18] MATLAB/Simulink Documentation. Available: http://www.mathworks.com

[19] Sreedhar Reddy Guda, "Modeling and Power Management of a Hybrid Wind-Microturbine Power Generation System" masters thesis in electrical engineering, Montana State University, Bozeman, Chap 4, July 2005.